Research Square

Preprints are preliminary reports that have not undergone peer review.
They should not be considered conclusive, used to inform clinical practice,
or referenced by the media as validated information.

A Novel Prognostic Model for Hepatocellular Carcinoma Patients Based on Signature Ferroptosis-Immune Microenvironment-Related Genes

Xisheng Yin
Southwest Medical University
Jiayi Tang
Southwest Medical University
Qian Yang
The First Affiliated Hospital of Chongqing Medical University
Ke Xu
Chongqing General Hospital
Shi Chen
The First Affiliated Hospital of Chongqing Medical University
Miao He
Laboratory Animal Center of Chongqing Medical University
Yuhan Yang
The First Affiliated Hospital of Chongqing Medical University
Jincheng Luo
Southwest Medical University
Yunyue Li
Medical School of Nanchang University
Xiaoyu Wang
Southwest Medical University
Xin Liu
Affiliated Hospital of Southwest Medical University
Hao Chi
Southwest Medical University
Xiaosong Li (lixiaosong@cqmu.edu.cn)
The First Affiliated Hospital of Chongqing Medical University

---

Research Article

Keywords: Hepatocellular carcinoma, Ferroptosis, Immune microenvironment, Prognosis

Posted Date: July 25th, 2022

DOI: https://doi.org/10.21203/rs.3.rs-1841506/v1

License: This work is licensed under a Creative Commons Attribution 4.0 International License.
Read Full License

Abstract

Background

Hepatocellular carcinoma (HCC) is one of the leading malignancies in the world due to its progressively increasing incidence. Nonetheless, the impact of ferroptosis and immune microenvironment on prognosis of HCC remains unclear. This research work aims to identify ferroptosis-immune microenvironment-related genes (FIMRGs) which influence the prognosis of HCC, providing a theoretical basis for an in-depth understanding of the pathogenesis and prognosis of HCC.

Methods

TCGA-LIHC cohort and GSE14520 cohort were enrolled in this study. 167 ferroptosis-related genes (FRGs) were retrieved from the FerrDb data resource. Consensus clustering assessment, immune infiltration assessment, weighted gene co-expression network analysis (WGCNA), Pearson correlation analysis along with Cox regression were used to identify and establish FIMRGs signature in HCC. Univariate coupled with multivariate regression assessment were executed to ascertain the independent prognostic worthiness of the risk score. The tumor microenvironment (TME) and drug sensitivity profiling were compared between the high-HCC risk and low-HCC risk groups. Subsequently, the drugs or molecular compounds targeting each prognostic gene were predicted via the DGIdb database.

Results

Based on 15 DEFRGs related with prognosis in individuals with HCC, the two clusters with significant prognostic differences have been mined. 9 genes (PTPRO, CRHBP, HMOX1, FABP5, TREM2, ADAMTS14, LILRA6, CAPG, and RGS2) have been identified from 55 FIMRGs, which were adopted to generate and verify the risk score model in the training along with the validation set. Cox regression assessment manifested the risk score to be independent predictive factor. TME analysis and drug sensitivity profiling exhibited remarkable differences in the immune microenvironment between high-HCC and low-HCC risk groups, with the low-HCC risk group being more likely to benefit from chemotherapy. Furthermore, A miRNA-mRNA regulatory network consisting of four prognostic genes and five prognostic miRNAs was formed. Finally, there were four drugs targeting HMOX1, one drug targeting RGS2, CAPG and CRHBP respectively, which have been extracted from the DGIdb database.

Conclusion

This study proposed a novel and promising prognostic gene signature, which could provide us a panoramic view of the prediction of prognosis for HCC patients.

Introduction

Owing to its ultra-high morbidity along with mortality, HCC is still one of the most deadly cancers globally [1, 2]. Most HCC patients are in late stages when they are detected, and the intricate background of liver disease, as well as the high relapse rate, are major variables influencing HCC therapy and prognosis. Although various novel medicines for advanced liver cancer, particularly targeted therapies, have been established in recent years, they have enhanced the overall survival of subjects with liver cancer. Nonetheless, further progress is necessary for the selection of people to benefit from specific molecular treatments, the identification of appropriate medicines, and the evaluation of clinical effectiveness[3]. Immunotherapies, especially immune checkpoint inhibitors, have provided new hope for the treatment of liver cancer, but comparable problems persist [4, 5]. Therefore, it is still critical to conduct a complete investigation of the mechanisms of liver cancer onset and progress, as well as to propose new perspectives to resolve the therapeutic conundrum.

Ferroptosis constitutes a newly recognized kind of programmed cell death triggered mostly by iron-induced oxidative damage, lipid hyper-peroxidation along with cell membrane degradation [6, 7]. Iron buildup along with peroxidation of lipids are both indicators of ferroptosis development, and modulation between oxidative damage and anti-oxidant defense is a critical molecular process of ferroptosis [7, 8]. Ferroptosis has been proven to play a very significant role in digestive system tumors, for instance pancreatic cancer, gastric cancer, colorectal cancer, and particularly liver cancer[9]. Notably, Gao et al. discovered that YAP / TAZ and ATF4 synergistically promoted the expression of antioxidant pathway-related genes, which in turn prevented ferroptosis and induced sorafenib resistance in HCC patients[10]. These insights provide a new strategy for anti-cancer therapy targeting ferroptosis.

Notably, there is growing evidence of a cross talk of ferroptosis with the TME. For example, CD8 + T cells potentially downregulate the expression of SLC3A2 and SLC7A11 to enhance ferroptosis, which promotes the antitumor efficacy of immunotherapy, indicating that the immune system may work, at least in part, via ferroptosis.[11, 12]. Furthermore, cancer cells undergoing ferroptosis may emit signals that affect anti-tumor immunity, such as oxidized lipid mediators, or a small minority of cells may inhibit the immune system, allowing tumor growth[12].

However, to date, it is unclear how the cross-talk of ferroptosis with immune microenvironment in HCC affects the onset and progress of HCC. Therefore, this work aimed to identify the prognostic worthiness of ferroptosis-immune cell infiltration-linked genes in HCC and the associated molecular mechanisms, to gain insight into the pathogenesis of HCC, and provide new strategies for targeted therapy of HCC.

Materials And Methods

2.1 Data source

The TCGA-LIHC cohort was abstracted from the TCGA data resource (https://portal.gdc.cancer.gov/), which included the sequencing data of 374 HCC samples and 50 non-tumorous samples. Of these, 370

HCC samples with complete clinical data were used as the training set. Comprehensive clinical information of the 370 samples was listed in **Table 1**. The GSE14520 cohort was abstracted from the GEO data resource (https://www.ncbi.nlm.nih.gov/geo/), which is composed of 255 HCC samples and 220 control samples. Among them, 221 HCC samples with complete clinical data were served as the validation set for the risk score model. The clinical information of GSE14520 cohort was listed in Table 2. 167 FRGs were abstracted from the FerrDb data resource.

Table 1

Clinical features of subjects in the TCGA-LIHC cohort.

Characteristic		N=370
Gender, n (%)	Female	121 (32.7%)
	Male	249 (67.3%)
Clinical stage, n (%)	Stage I	171 (49.4%)
	Stage II	85 (24.6%)
	Stage III	85 (24.6%)
	Stage IV	5 (1.4%)
T stage, n (%)	T1	181 (49.2%)
	T2	93 (25.3%)
	T3	80 (21.7%)
	T4	14 (3.8%)
N stage, n (%)	N0	252 (98.4%)
	N1	4 (1.6%)
M stage, n (%)	M0	266 (98.5%)
	M1	4 (1.5%)
Vital status, n (%)	Alive	239 (64.6%)
	Dead	131 (35.4%)
Age, median (IQR)		61 (51.25, 69)

Table 2

Clinical features of subjects in the GSE14520 cohort.

Characteristic		N=221
Gender, n (%)	Fmale	29 (13.1%)
	Male	192 (86.9%)
TNM stage, n (%)	I	93 (42.1%)
	II	78 (35.3%)
	III	50 (22.6%)
AFP (>/<=300ng/ml), n (%)	High	100 (45.2%)
	Low	121 (54.8%)
Vital status, n (%)	Alive	136 (61.5%)
	Dead	85 (38.5%)
Age, median (IQR)		50 (44, 58)

2.2 Determination of differential expressed genes (DEGs) and miRNAs (DE-miRNAs)

The DEGs and DE-miRNAs between non-tumorous and HCC samples in the TCGA-LIHC cohort were assessed with the R 'limma' package[13]. The cut-off criterion was $|\log_2 \text{FoldChange(FC)}| > 1$ along with a adjusted p-value < 0.05. The corresponding volcano maps and heatmaps were created via the R 'ggplot2' package and R 'pheatmap' package respectively. The differential expressed ferroptosis-related genes (DEFRGs) were authenticated by overlapping the DEGs and 167 FRGs. The corresponding Venn diagram was plotted by the JVENN web resource (http://jvenn.toulouse.inra.fr/app/example.html) [14].

2.3 Unsupervised clustering

DEFRGs associated with prognosis were picked out via univariate Cox assessment. On the basis of the expression of DEFRGs associated with prognosis, 370 HCC cases from the TCGA-LIHC cohort were classified by consensus clustering algorithm through the 'pam' algorithm in the R 'ConsensusClusterPlus' package[15].

2.4 Functional and pathway enrichment analysis

Gene Set Variation Analysis (GSVA) was carried out using the R "GSVA" package to identify different pathways between different ferroptosis clusters and to analyze differences in their biological functions[16]. The 'c2.cp.kegg.v7.4.-symbols' gene set was abstracted from the MSigDB data resource to perform GSVA enrichment analysis. Significant differences were signified by $P< 0.05$. Gene Ontology (GO) along with Kyoto Encyclopedia of Genes and Genomes (KEGG) enrichment analysis were implemented through the R 'clusterProfiler' package[17]. The significance threshold is p-value < 0.05. GO comprised the biological processes (BP), cellular components (CC), along with molecular functions (MF) related with genes. KEGG analysis uncovered biological pathways associated with genes.

2.5 Invading immune cells analysis

To better comprehend the immune micro-environment of individuals with HCC, we used single sample gene set enrichment analysis (ssGSEA) to assess the relative fraction of immune cells as well as immune features on the basis of the gene expression matrix along with gene set of immune cell subgroups present in the official website.

2.6 Weighted gene co-expression network analysis (WGCNA)

The expression data of the TCGA-LIHC cohort was analyzed through the R 'WGCNA' package[18] to generate the WGCNA co-expression network with infiltrating immune cells and immune features as clinical traits. The 'goodSamplesGenes' function was used to perform sample clustering to identify and remove outliers. To make the co-expression network satisfy the distribution of scale-free network, a soft-thresholding power was computed with the pickSoftThreshold function. The dynamic tree cutting method was utilized to recognize different modules harboring a minimum number of 100 genes per module. Subsequently, the merging threshold was set at 0.45 to merge similar modules. These modules were further analyzed for correlation with infiltrating immune cells. Lastly, the module harboring the highest Pearson correlation with infiltrating immune cells and immune features was selected for subsequent analysis.

2.7 Generation and validation of the risk score model

The univariate Cox assessment was employed to assess genes that were remarkably linked to (p-value < 0.05) the survival of the HCC subjects in the training set. Subsequently, Multiple regression analysis of candidate genes was performed using a stepwise regression function to obtain the optimized regression equation and the corresponding coefficients of prognostic gene. The risk score calculating formula was: Risk score = $\sum_{1}^{n} \mathrm{coef}\left(\mathrm{genei}\right) * \mathrm{expr}\left(\mathrm{genei}\right)$, where coef is the regression coefficient, expr represented the expression value of prognostic genes.

To stratify patients into high-HCC and low-HCC risk groups, the median of the risk score was determined. Overall survival (OS) between the high-HCC and low-HCC risk groups was assessed by the "survminer" R software package, using K-M survival curves and log-rank tests. Besides, the area under the curve (AUC) of receiver operating characteristic (ROC) was computed using the R 'survival ROC' package. In addition, the risk plot was generated via the R 'pheatmap' resource. We used the GSE14520 cohort as the validation cohort. The above procedure was carried out in the training set and validation set respectively to construct and verify the risk score model.

2.8 Independent prognostic assessment

To establish the risk score independent prognostic worthiness, univariate along with multivariate regression assessments with the risk score and major clinicopathological variables (age, stage, sex, AFP) were performed. Statistical significance was deemed at p< 0.05.

2.9 TME and drug sensitivity analysis

The TME is closely linked to the onset and progress of HCC. According to Charoentong et al' study[19], the Pearson coefficient was used to explore the correlation between nine FIMRGs and 121 immunomodulators including MHC, receptors, chemokines, and immunostimulants. The CIBERSORT algorithm[20] was used to contrast the differences in proportions of diverse immune cells among different risk populations. In addition, we obtained the cancer-immune cycle-related gene set [19] from the website (http://biocc.hrbmu.edu.cn/TIP/) developed by Xu et al. A set of genetic characteristics which are positively related with clinical response to anti-PD-L1 drug (atezolizumab) was obtained from Mariathasan's study[21]. The ssGSEA was adopted to assess cancer immune cycle and immunotherapy-related gene set enrichment scores between high-HCC and low-HCC risk groups, and the differences were deemed significant at $P< 0.05$. Lastly, we gathered 22 suppressive immune checkpoints harboring therapeutic worthiness from Auslander's study[22].

The R 'pRRophetic' package is used to analyze drug sensitivity in high-HCC and low-HCC risk populations. Drug sensitivity is expressed as an IC50 value. IC50 is defined as the semi-inhibitory concentration.

2.10 Multi-Omics analysis of prognostic genes

Exome sequencing data, copy number variation data, and methylation profiles were acquired from the TCGA GDC portal. The website GSCALite[23] (http://bioinfo.life.hust.edu.cn/web/GSCALite/) was utilized for the multi-omics analysis of prognostic genes.

2.11 Establishment of a prognostic miRNA-mRNA regulatory network

To assess the regulatory mechanisms associated with this risk prediction model, we established a miRNA-mRNA modulatory network. We first identified the DE-miRNAs between HCC and non-tumorous samples in the TCGA-LIHC cohort. The miRNAs associated with prognostic genes were then predicted by the miRbase database (http://mirdb.org/). The intersecting miRNAs were enrolled in a univariate Cox analysis to obtain prognostic miRNAs. The final prognosis-associated network of miRNA-mRNA was visualized via the Cytoscape software[24].

2.12 Prediction of potential drugs

The DGIdb database (https://dgidb.org/search_interactions) was employed for searching the drugs or molecular compounds targeting each prognostic gene[25]. The drug-gene interaction network was visualized using Cytoscape[24].

2.13 Protein levels of FIMRGs in HPA database

The human protein atlas (HPA) is a database (https://www.proteinatlas.org/), containing immunohistochemical staining images of about 20 most common cancer types, the protein expression levels of nine genes in normal liver and HCC tissues were verified using HPA database [26].

2.14 Statistical analysis

All analyses were executed by the R programming language, and the data from different groups were compared by the Kruskal–Wallis test or Wilcoxon test. If not specified above, a P< 0.05 indicated statistical significance.

Results

3.1 Identification of ferroptosis-related subtypes in HCC

To mine the DEFRGs between HCC and normal samples, we first screened the DEGs between HCC and non-tumorous samples in the TCGA-LIHC cohort. As shown in Fig. 1A and **Supplementary Table 1, 5622** DEGs were filtrated on the basis of the criteria of $|\log_2(FC)| > 1$ along with adjusted p-value < 0.05, including 2462 up-regulated genes, as well as 3160 down-regulated genes. The TOP100 DEGs were displayed in Fig. 1B. We then took the intersection of 5622 DEGs and 167 FRGs to obtain 36 DEFRGs (Fig. 1C). The above 36 genes were further included in the univariate Cox assessment and 15 genes relevant to overall survival (OS) in individuals with HCC ($p < 0.05$) were identified, namely STMN1, MAFG, TXNIP, SLC7A11, RRM2, PCK2, MT3, IL33, HMOX1, GPT2, CBS, CAPG, AURKA, ASNS and ALB (Fig. 1D). We analyzed the Pearson correlations between these 15 genes. The results showed a positive correlation between STMN1 and RRM2, STMN1 and AURKA, SLC7A11 and MAFG, RRM2 and AURKA, PCK2 and GPT2, and PCK2 and ALB (Fig. 1E). To further understand the interactions between the proteins encoded by these 15 genes, we constructed a PPI network containing 13 nodes with 16 edges (Fig. 1F).

To explore the ferroptosis-related subtypes in HCC, 370 HCC samples were clustered using unsupervised cluster analysis based on the expression of 15 DEFRGs. Two subtypes, cluster 1 along with cluster 2, were identified from the results (Fig. 2A). Cluster 1 included 140 cases and cluster 2 included 230 cases. Survival analysis exhibited remarkable differences in prognosis between the two ferroptosis-related subtypes, and cluster 2 had a decent survival advantage (Fig. 2B). To further explore possible mechanisms of the survival differences between the two clusters, GSVA enrichment assessment was conducted on these two subtypes to assess the differences with regard to function along with pathways. The results manifested that cluster 1 was abundant in oncogenic cascades, consisting of the P53 signaling cascade, and some metabolic cascades (Fig. 2C). Cluster 2 was primarily enriched in glucose metabolic cascades and immune-related cascades, consisting of PPAR signaling cascade and adipocytokine signaling cascade (Fig. 2C).

3.2 FIMRGs in HCC

We then compared the infiltrating immune cells and immune features in Cluster 2 and Cluster 1 using ssGSEA. The results manifested that the enrichment fraction of most immune cells and immune features was greater in cluster 1 compared to cluster 2 (**Fig.2D**). The correlation between the different immune cells and immune features was shown in **Fig.2E**. To assess further the genes linked with the immune micro-environment, we included the above infiltrating immune cells and immune features into the WGCNA analysis. No obvious outliers were excluded by cluster analysis (**Fig.3A**). 5 was selected as the optimal

soft threshold with an R^2 = 0.85 (**Fig.3B**). On the basis of the optimal soft threshold, we stratified the genes into different modules according to the dynamic tree-cutting algorithm. After merging, a total of 7 modules were generated (**Fig.3C**). Correlations of the modules with traits were computed and brown modules were associated with most traits as key modules (**Fig.3D**). The 1436 genes in key module were defined as immune microenvironment-linked genes in HCC. To further identify FIMRGs, we assessed the relationships of the 1436 immune microenvironment-linked genes with the 15 prognosis-linked DEFRGs. After selecting the relationship pairs with correlation coefficient > 0.5 along with p-values < 0.05, the corresponding genes were combined and de-duplicated to finally obtain 55 genes defined as FIMRGs in HCC (**Supplementary Table 2**).

To investigate further the biological functions of the above 55 genes and the involved pathways, GO and KEGG enrichment analysis was carried out. A total of 291 GO items (including 279 BP items, 7 CC items and 5 MF items) and 10 KEGG pathways were enriched (**Supplementary Table 3**). Top5 GO entries under each category were listed in **Fig.3E**. We established that these 55 genes were most linked with 'immune response-modulating signaling cascade', 'immune response-modulating cell surface receptor signaling cascade', 'activation of immune response', 'immune response-activating cell surface receptor signaling cascade', and 'immune response-activating signal transduction'. In addition, for KEGG pathways, these 55 genes were enriched in 'Osteoclast differentiation', 'Neutrophil extracellular trap formation', 'C-type lectin receptor signaling cascade', 'HIF-1 signaling cascade', 'Ferroptosis', 'Phagosome', 'Chemokine signaling cascade', 'Rap1 signaling cascade', and 'B cell receptor signaling cascade' (**Fig.3F**).

3.3 Creation and verification of the risk score model based on FIMRGs in HCC

In the following, the univariate Cox assessment was fulfilled to identify prognosis-linked genes on the basis of 55 FIMRGs in the training set. Nine out of the 55genes were identified as closely related to patients' OS in the training set **(Fig.4A)**. Then, the nine genes were submitted further to stepwise multivariate Cox regression assessment. These 9 FIMRGs (PTPRO, CRHBP, HMOX1, FABP5, TREM2, ADAMTS14, LILRA6, CAPG, and RGS2) were identified as prognostic genes and each regression coefficient was determined. Then we generated a risk score model. To assess the availability of the model, the patients were split into high-HCC and low-HCC risk groups on the basis of the median of the risk score in the training data set. Then K-M survival analysis was performed. The results suggested that patients in high-HCC risk group had remarkably worse survival rates versus those in low-HCC risk group **(Fig.4B)**. The AUC value of the ROC curve in the training cohort was 0.646, exhibiting a decent accuracy (**Fig.4C**). **Fig.4D** displayed the ranked risk scores along with the survival status of individual patients in the training cohort. The distribution map of survival status revealed that patients suffered a greater mortality risk with increasing risk scores. The expression of nine prognostic genes in low-HCC and high-HCC risk groups was exhibited in **Fig.4E**. The heatmap results suggested PTPRO, HMOX1, FABP5, TREM2, ADAMTS14, LILRA6, CAPG, and RGS2 were highly expressed in the high-HCC risk group. CRHBP was highly expressed in the low-HCC risk group.

We utilized an independent data set with 221 HCC subjects from the GSE14520 to prove the accuracy of the model externally. Consistent with the TCGA-LIHC cohort, subjects with high-HCC risk exhibited worse OS in the validation set (**Fig.4F**). Correspondingly, the AUC value of the ROC curve in predicting prognosis was 0.624 (**Fig.4G**). **Fig.4H** exhibited the survival status on the basis of the patients with increased risk scores and the heatmap result suggested that PTPRO, HMOX1, FABP5, TREM2, ADAMTS14, LILRA6, CAPG, and RGS2 were highly expressed in the high-HCC risk group (**Fig.4I**). CRHBP was highly expressed in the low-HCC risk group (**Fig.4I**). These results further affirmed the validity of our risk model in forecasting the survival of HCC patients. Taken together, these results demonstrated that FIMRGs were associated with the prognosisi of HCC.

3.4 Independent prognostic worthiness of the risk score based on FIMRGs in HCC

To clarify the role of the gene signature in HCC progression, we researched the correlation of the risk score with clinical characteristics in the training set. As indicated in **Fig.S1A**, the risk score was linked with stage. The expression of prognostic genes under different clinical factors and our risk score distribution of patients with different clinical features in the training set, as well as the verification set were shown in **Fig.S1B-C**. Subsequently, we conducted univariate along with multivariate Cox regression assessments to assess if the risk score was independent of other clinical parameters (age, stage, gender, and AFP) as a predictive factor for individuals with HCC in the training set and verification set respectively. The univariate assessment exhibited that the stage and risk score was relevant to patients' prognosis **(Fig.5A, 5C)**. The multivariate Cox regression assessment demonstrated that the risk score could be used independently to estimate the survival of patients **(Fig.5B, 5D)**. Furthermore, to predict the survival outcome of HCC, a prognostic nomogram was established through Cox regression model analysis according to two significant indepentent indicators (stage and risk score) **(Fig.S3A-D**). The C-index value was 0.682 in the training set and 0.636 in the validation set. The time-dependent AUC was > 0.6 for the prediction of OS within 5 years in both the training and validation cohorts, indicated relatively good discrimination by the nomogram. Then, We plotted the ROC curves (**Fig.S3E-F**)

3.5 Differential analysis of TME and sensitivity to chemotherapy in high-HCC and low-HCC risk groups

We detected that nine FIMRGs were positively correlated with many immunomodulators (**Fig.S2A**). Expression of MHC was strongly correlated with antigen presentation and processing capacity. Chemokines along with their receptors facilitate the mobilization of effector TIICs, consisting of CD8+ T cells, antigen-presenting cells, and TH17 cells. Exploring the relevance of nine FIMRGs to immune modulators aims to elucidate the immune role of nine genes in TME.

To explore possible mechanisms for the disparity in prognosis between the high-HCC and low-HCC risk groups, we first performed an analysis of infiltrating immune cells (**Fig.6A-B**). The data revealed that the relative abundance of memory B cells, CD4 Memory T cells, follicular helper T cells, Macrophages (M0), as well as regulatory T cells (Tregs), was remarkably greater in the high-HCC risk group compared to the low-HCC risk group (**Fig.6C**). Meanwhile, the relative abundance of naive B cells, Monocytes, resting memory CD4+T cells, Macrophages (M1), activated NK cells, Macrophages (M2), and resting Mast cells

was remarkably lower in the high-HCC risk group compared to the low-HCC risk group (**Fig.6C**). Hence, we speculated that there was a significant distinction in the immune microenvironment between the high-HCC and low-HCC risk groups.

The activity of the cancer-immune cycle is a straightforward and integrated expression of the function of the chemokine system as well as other immunoregulators[24, 27], and the activity of these steps determines the fate of tumor cells. In the high-HCC risk group, the activity of all steps of the immune cycle was found to be upregulated (**Fig.6D**), including seven steps: cancer cell antigen release (step 1), cancer antigen presentation (step 2), initiation and activation (step 3), immune cell moving toward the tumor (step 4) (CD8 T-cell mobilization, macrophage mobilization, Th1 cell mobilization, NK cell mobilization, DC mobilization, and recruitment of TH17), immune cell invasion into the tumor (step 5), T cell recognizing of cancer cells (step 6) along with killing cancer cells (step 7). All of these showed a higher immune infiltration status in the high-HCC risk group. Theoretically, patients in the high-risk group should have a higher response to immunotherapy because subjects in the high-HCC risk group have an inflammatory TME. Subsquently, we used Tumor Immune Dysfunction and Exclusion (TIDE) (http://tide.dfci.harvard.edu/) to predict immunotherapy response in the high-risk and low-risk groups, and additionally used the submap module in GenePattern Modules (https://www.genepattern.org/modules) using data from melanoma as a template . The similarity between the high-risk and low-risk groups and the two immune checkpoint inhibitor treatment data was predicted. It was found that the predicted TIDE scores were significantly higher in the high-risk group than in the low-risk group, and the data from the high-risk group were significantly similar to the data from the PD1 treatment response group (Fig.S4).

Next, we contrasted the expression of 20 important immune checkpoints between the high-HCC and low-HCC risk groups, the expression of 17 immune checkpoints were remarkably different. As exhibited in **Fig.6E**, the expression of PD-L1, TIM-3, PD-1, CTLA-4, as well as LAG-3 were remarkably higher in the high-HCC risk group, and only the expression of ADORA2A was decreased, indicating that the high-HCC risk group might have a better response to immune checkpoint inhibitors.

As expected, the enrichment scores for all immunotherapy-positive genetic characteristics were higher in the high-HCC risk group (**Fig. 6F**). In addition, we further analyzed the sensitivity of high-HCC and low-HCC risk groups to drugs. As revealed in **Fig.6G**, the low-HCC risk group was more sensitive to five chemotherapy drugs (Axitinib, Rapamycin, Temsirolimus, Docetaxel, and Metformin), suggesting that patients in the low-HCC risk group would benefit more from chemotherapy.

3.6 Multi-Omics analysis of prognostic genes

As exhibited in **Supplementary Table 1**, the expression of PTPRO, CRHBP, HMOX1, LILRA6, and RGS2 was reduced in HCC tissues, and the expression of TREM2, FABP5 and ADAMTS14 was up-regulated in HCC tissues. To assess further the biological mechanisms underlying the aberrant expression of prognostic genes in HCC tissues, we performed a multi-omics analysis of these genes. 8 genes were mutated in HCC tissues, mainly missense mutations (**Fig.7A**). As these eight genes presented differential expression in

most HCC samples, we hypothesized that the aberrant expression of prognostic genes was not mutation-related. We further investigated the abnormal methylation levels. As shown in **Fig.7B**. TREM2 was hypermethylated in HCC tissues. Aberrant methylation is known to play an instrumental role in the modulation of expression levels, so we then analyzed the relevance between methylation levels and expression levels. The result indicated that methylation of TREM2 was not correlated with the expression (**Fig.7C**). Next, we contrasted copy number variation (CNV) in terms of both heterozygosity and homozygosity. As revealed in **Fig.7D-E**, we detected the presence of amplified variants in the RGS2, FABP5, and TREM2. Nevertheless, there was no remarkable correlation between CNV and expression level variation in RGS2, FABP5, and TREM2 (**Fig.7F**). Therefore, we hypothesize that the aberrant expression regulation of prognostic genes in HCC does not occur at the genomic level and requires further investigation.

3.7 Establishment of a prognosis-related miRNA-mRNA regulatory network

We then explored the post-transcriptional regulatory mechanisms of prognostic genes. First, we analyzed the DE-miRNAs between HCC samples and normal samples. A total of 399 DE-miRNAs, containing 156 up-regulated miRNAs and 234 down-regulated miRNAs, were identified (**Supplementary Table 4, Fig.8A**). Top100 DE-miRNAs were shown in the heatmap (**Fig.8B**). Through the miRbase database, we obtained 67 miRNAs associated with prognostic genes. 13 DE-miRNAs associated with prognostic genes were acquired after intersecting with DE-miRNAs (**Fig.8C**). 5 miRNAs linked with the overall survival of individuals with HCC were further authenticated by univariate Cox analysis (**Fig.8D**). We finally constructed a miRNA-mRNA regulatory network comprising four prognostic genes and five prognostic miRNAs (**Fig.8E**). In the network, the hsa-miR-642a-5p regulated the expression of HMOX1 and PTPRO. The hsa-miR-1304-5p regulated the expression of HMOX1. The hsa-miR-133b regulated the expression of PTPRO. The hsa-miR-125a-5p regulated the expression of ADAMTS14. The hsa-miR-3162-5p regulated the expression of RGS2.

3.8 The potential drugs targeting the prognostic genes

To further explore potential drugs targeting prognostic genes, we extracted four drugs targeting HMOX1 from the DGIdb database, including ASPIRIN, STANNSOPORFIN, SUNITINIB, and SORAFENIB. In addition, one drug targeting RGS2, HALOPERIDOL, and one drug targeting CAPG, VINCRISTINE were also identified. We also discovered that ALCOHOL targeted CRHBP (**Fig.8F**).

3.9 FIMRGs differentially express in protein level

In HPA, the histological expression of FIMRGs in normal and tumor tissues was shown in **Fig.9**. There were significant differences in the expression of three genes at the protein level between normal and liver cancer tissues. The protein expressions of FABP5, TREM2 and CAPG were significantly up-regulated. However, no significant expression differences were found in PTPRO, CRHBP and HMOX1. The protein expressions of PTPRO, CRHBP and HMOX1 were lower in normal and tumor tissues. ADAMTS14, LILRA6 and RGS2 failed to find data in the database.

Discussion

Ferroptosis, a unique mode of programmed cell death, is closely linked with the development and occurrence of HCC. Yao et al. found that in HCC, LIFR and SHP1 synergistically activate the NF-κB signaling cascade and upregulate LCN2 (iron-draining cytokine), leading to iron depletion and ferroptosis agonist insensitivity[28]. In Huh7, snu-449, as well as snu-182 HCC cell lines, Li et al. discovered that artesunate increased the anticancer influences of low-dose sorafenib, and that this effect was caused by activation of ferroptosis in HCC cells.[29]. With the intensive study of the tumor microenvironment, the interaction between ferroptosis and immune microenvironment has been identified. As a key ferroptosis modulator, HMGB1 can participate in tumor immunity via the RAS-JNK / p38 cascade [30]. Through the downregulation of SLC7A11 and SLC3A2 expression, activated CD8 T lymphocytes increase ferroptosis-distinct lipid peroxidation in tumor cells[11]. In vitro and in vivo, anti-PD-L1 monoclonal antibodies along with ferroptosis activators, for instance erastin, RSL3, and cyst(e)inase work together to inhibit tumor growth[31]. However, it is unclear how the cross talk between ferroptosis and immune microenvironment in HCC affects the development of HCC.

Herein, we identified a total of 55 FIMRGs, and GO and KEGG analyses revealed that such genes may be implicated in regulating ferroptosis signaling pathways and various immune-related signaling pathways, such as Neutrophil extracellular trap formation, Chemokine signaling pathway, etc. According to previous reports, Neutrophil extracellular traps (NETs) can awaken dormant cancer cells, leading to tumor relapse, and unrestricted proliferation and spread. NETs serve a vital regulatory function in the tumor microenvironment, exerting many pro-tumor effects at various stages of tumor development[32]. Fabio summarized chemokines along with their receptors can similarly contribute to the pathogenesis of HCC, promoting cancer cell proliferation, tumor inflammatory microenvironment, immune response evasion, and angiogenesis[33]. Hence the enrichment of GO and KEGG confirms the biological significance of FIMRGs in immune regulation.

A nine-gene signature model associated with the ferroptosis-immune microenvironment in a huge HCC cohort have been identified, which included a training and validation dataset, and investigated the model's association with prognosis and immune infiltration in the HCC population. A promising strategy is provided to guide individualized treatment and improve prognostic prediction with clinical importance. Besides, the biological functions of these nine genes in human cancer pathology have been confirmed in several independent reports. Reduced PTPRO expression diminished T cell mediated immunity against tumors and remarkably promoted the proliferation of HCC in mice[34]. In addition, Zhang et al. found that IL-6 and PTPRO, in HCC, were jointly involved in regulating the expression of PD-L1 in monocytes and macrophages[35]. And PTPRO has been implicated as a carcinogenic factor in several malignancies, like colorectal cancer and breast cancer [35, 36]. CRHBP was found to be lowly expressed in HCC, and Wang et al. established that CRHBP could retard HCC progression by reducing cell cycle protein B2 expression and impairing cell cycle protein B2-CDK1[37]. Yang et al. study confirmed that CRHBP was able to inhibit the progression of renal hyaluronic cell carcinoma by modulating the inflammatory response and apoptosis[38]. Jiang et al. established that HMOX1, a downstream gene of miRNA-15a-3p, was over-

expressed in HCC, and over-expression of HMOX1 was detrimental to the prognosis of HCC[39]. A recent investigation exhibited that in tumor-associated macrophages, high expression of HMOX1 promoted tumor metastasis by promoting tumor angiogenesis, macrophage M2 polarization, repression of CD8 + T cells and epithelial-to-mesenchymal transition[40]. In addition, HMOX1 has been shown to induce ferroptosis through cell redox regulation and iron accumulation. For example, HMOX1 is a key mediator of BAY-induced ferroptosis [41], and EF24 can induce ferroptosis by raising HMOX1 expression[42]. Liu et al. found by single-cell transcriptomic assessment that FABP5 mediates tumor immunity in CD137-rich exhausted T-cells and that FABP5 may be a potential immune-metabolic marker for HCC[43]. Besides, Xu et al. found that activation of the FABP5/HIF-1 axis was involved in mediating lipid build-up and cell proliferation in HCC cells[44]. FABP5 is noted to be expressed in T cells and FABP5 caused mitochondrial changes that triggered mtDNA release, which in turn led to enhanced production of IL-10 and promoted Treg suppressive activity[45]. TREM2 expression was upregulated in HCC, and TREM2 prevents hepatocyte proliferation and injury, thereby suppressing HCC development and growth. Esparza-Baquer A et al. hypothesized that hepatic TREM2 agonists may attenuate liver injury, inflammatory response and oxidative stress in HCC[46]. In addition, TREM2 was shown to be a pro-tumorigenic marker of tumor-infiltrating macrophages that could target tumor growth inhibition and improve the efficacy of checkpoint blockade therapy, while regulating the landscape of remodeled tumor-infiltrating macrophages[47]. Song et al. showed that ADAMTS14 may inhibit HCC progression by regulating miR-572 / RCAN1 as a competitive endogenous RNA.CAPG has been documented to participate in the onset and progress of HCC[48], breast cancer[49], glioma[50], colorectal cancer[51] and bladder cancer[52]. Studies of RGS2 and LILRA6 in HCC have not been reported. However, RGS2 has been demonstrated to support the proliferation of slow-cycle/dormant cancer cells (SCCs) through mediating the expression of ATF4, and thus facilitate cancer relapse and drug resistance[53]. Yang et al. discovered that in breast cancer, drugs diminished proliferation, metastasis and differentiation of breast cancer cells by activating RGS2-targeted calcium signaling [54]. In addition, copy number variation of LILRA6 was reported to be associated with susceptibility to nasopharyngeal carcinoma[55].

The cancer immune cycle represents our body's immune response to cancer. The activity of the cancer-immune cycle holistically reflects the ultimate effect of the complicated immunomodulatory cross talks in TME. Here, we noticed that all immune step scores appear upregulated in the high-HCC risk group. Thus, individuals in the high-HCC risk group had an inflammatory TME. A previous phase I clinical trial exhibited that Tremelimumab (CTLA4 blocker) had a controllable safety profile with an efficiency of 17.6% in 17 patients with HCV-associated advanced HCC[56]. In addition, in a phase ½ clinical trial, Nivolumab (PD-1 blocker) showed an objective remission rate of 20% and an overall survival rate of 67% during the dose extension period in 214 subjects with advanced HCC[57]. More recently, a study reported significant improvements in postoperative survival overall along with progression-free survival in subjects with primary HCC not amenable to surgical resection after combined treatment with cintilizumab-bevacizumab biosimilar and sorafenib[58]. These studies demonstrate the effectiveness and reliability of immune checkpoint blockade in HCC patients, and the advent of immunotherapy has provided new ideas for the treatment of HCC. Previous investigations have shown elevated expression of PD-1[59–61],

TIM3[62] and LAG3[63] on CD4 + or CD8 + tumor infiltrating lymphocytes in HCC patients. Another key feature of inflammatory TME is the upregulation of suppressive immune checkpoints. In our research, the suppressive immune checkpoints were remarkably upregulated in the high-HCC risk group, along with a generally elevated enrichment score for immunotherapy prediction cascades, indicating that high-HCC risk subjects have a higher immune infiltration status. Furthermore, tumor-infiltrating lymphocyte-mediated ferroptosis has been documented to promote the effectiveness of immune checkpoint inhibitors. In HCC treatment, it is believed that iron overload in cancer cells enhances immune checkpoint blockade, which stimulates the build-up of reactive oxygen species and sensitizes cancer cells to iron sagging[64, 65]. Thus, ferroptosis-immune microenvironment-related genetic characteristics may provide potential clues for patients' selection of more effective antitumor immunotherapies.

Genetic alterations are important in controlling gene expression and cancer progression [66]. Genome-wide assessment of genes exhibited that DAMTS14 had the highest frequency of mutations. DNA methylation is a critical epigenetic modification that controls the expression of oncogenic or tumor suppressor genes. One study confirmed that hypomethylation levels of TREM2 could be a biomarker for the pathogenesis of Alzheimer's disease[67]. Although scientists have suggested the potential validity of methylation biomarkers in predicting the prognosis of HCC[68, 69], studies on the methylation of these ferritin-related genes in HCC are scarce, so it would be interesting to conduct further studies. In addition, amplification variants exist in RGS2 and TREM2. CNV burden has been reported to have an impact on the immune profile and molecular characteristics of HCC[70]. This suggests that CNV identification may be one of the promising directions for future anti-cancer therapy.

Through miRNA-mRNA network construction, we further identified five miRNAs related with the prognosis of individuals with HCC. We identified new miRNAs (miR-642a-5p and miR-1304-5p) associated with HMOX1 that regulate the progression of HCC. Ma et al. found that MiRNA-15a-3p inhibited HCC metastasis by interacting with HMOX1[39], thus confirming that miRNAs can influence the progression of HCC through mRNAs. Most HCC subjects were diagnosed at an advanced intermediate stage, during which effective treatments were limited, principally transarterial chemoembolization (TACE) along with targeted therapy with the multikinase inhibitor sorafenib[71]. Sorafenib is an effective targeted treatment modality for HCC[72, 73], but early resistance occurs in some patients, preventing long-term benefit. And some studies noted that knocking down the expression of HMOX1 remarkably diminished the anti-cancer effect of cefotaxime in CNE2 cells[74]. Our study identified four anticancer drugs targeting HMOX1, including sunitinib, sorafenib, aspirin, and stannsoporfin. Chi et al. indicated that miRNA could affect the chemosensitivity of HCC via mRNA[75]. Therefore, we hypothesized that HMOX1 could affect HCC drug resistance through the miRNA-mRNA network. Thus, although more investigations are needed to confirm the above ideas, these results could serve as a theoretical foundation for the development of safe and effective tumor-targeting drugs.

However, this study also has several limitations. Firstly, this research is primarily grounded in comprehensive bioinformatics, and currently lacks validated experimental verification of these findings.

Secondly, it is a retrospective analysis and more prospective investigations are pivotal to validate such results. However, we will continue to focus on the biological functions of these genes in tumors.

Conclusion

In this study, there were nine FIMRGs have been identified successfully that affect the prognosis of HCC patients, created corresponding risk score models, and explored the relationship between the models and TME, as well as the regulatory mechanisms and targeting agents of these prognostic genes. This research prospectively provides a new research target to explore the pathogenesis and progression of HCC patients and provides new insights to estimate the prognosis of HCC.

Declarations

Data Availability Statement

The datasets utilized in this investigation are available through online repositories. The article/Supplementary Material contains the repository/repositories names and accession number(s).

Conflict of Interest

None.

Author Contributions

XSL, XY and HC constructed the study. XY, SC, MH and JT performed the data analysis and drafted the manuscript. KX and QY performed the data analysis and plotted the figures. JL, YL and QY drafted and revised the manuscript. XW, JT and XL were in charge of data collection and critical reading of the manuscript. All authors contributed to manuscript revision, read, and approved the submitted version.

Funding

This study was funded by the Natural Science Foundation of Chongqing (cstc2020jcyj-msxmX0159, cstc2021jsyj-yzysbAX0018), Chongqing Science and Health Joint Medical High-end Talent Project (2022GDRC012), and Science and Technology Research Program of Chongqing Municipal Education Commission (KJZD-K202100402, KJQN201900449).

Acknowledgments

This is a brief acknowledgement of specific colleagues, institutions, or agencies that assisted the authors' efforts.

References

1. Llovet, J.M., et al., *Hepatocellular carcinoma.* Nat Rev Dis Primers, 2021. **7**(1): p. 6.

2. Singal, A.G., P. Lampertico, and P. Nahon, *Epidemiology and surveillance for hepatocellular carcinoma: New trends.* J Hepatol, 2020. **72**(2): p. 250-261.
3. Faivre, S., L. Rimassa, and R.S. Finn, *Molecular therapies for HCC: Looking outside the box.* J Hepatol, 2020. **72**(2): p. 342-352.
4. Heinrich, S., et al., *Understanding tumour cell heterogeneity and its implication for immunotherapy in liver cancer using single-cell analysis.* J Hepatol, 2021. **74**(3): p. 700-715.
5. Sangro, B., et al., *Diagnosis and management of toxicities of immune checkpoint inhibitors in hepatocellular carcinoma.* J Hepatol, 2020. **72**(2): p. 320-341.
6. Chen, X., et al., *Broadening horizons: the role of ferroptosis in cancer.* Nat Rev Clin Oncol, 2021. **18**(5): p. 280-296.
7. Dixon, S.J., et al., *Ferroptosis: an iron-dependent form of nonapoptotic cell death.* Cell, 2012. **149**(5): p. 1060-72.
8. Jiang, X., B.R. Stockwell, and M. Conrad, *Ferroptosis: mechanisms, biology and role in disease.* Nat Rev Mol Cell Biol, 2021. **22**(4): p. 266-282.
9. Deng, J., R.J. Sinard, and B. Murphy, *Patient experience of head and neck lymphedema therapy: a qualitative study.* Support Care Cancer, 2019. **27**(5): p. 1811-1823.
10. Gao, R., et al., *YAP/TAZ and ATF4 drive resistance to Sorafenib in hepatocellular carcinoma by preventing ferroptosis.* EMBO Mol Med, 2021. **13**(12): p. e14351.
11. Wang, W., et al., *CD8(+) T cells regulate tumour ferroptosis during cancer immunotherapy.* Nature, 2019. **569**(7755): p. 270-274.
12. Stockwell, B.R. and X. Jiang, *A Physiological Function for Ferroptosis in Tumor Suppression by the Immune System.* Cell Metab, 2019. **30**(1): p. 14-15.
13. Smyth, G.K., *Linear models and empirical bayes methods for assessing differential expression in microarray experiments.* Stat Appl Genet Mol Biol, 2004. **3**: p. Article3.
14. Bardou, P., et al., *jvenn: an interactive Venn diagram viewer.* BMC Bioinformatics, 2014. **15**(1): p. 293.
15. Wilkerson, M.D. and D.N. Hayes, *ConsensusClusterPlus: a class discovery tool with confidence assessments and item tracking.* Bioinformatics, 2010. **26**(12): p. 1572-3.
16. Hänzelmann, S., R. Castelo, and J. Guinney, *GSVA: gene set variation analysis for microarray and RNA-seq data.* BMC Bioinformatics, 2013. **14**: p. 7.
17. Yu, G., et al., *clusterProfiler: an R package for comparing biological themes among gene clusters.* Omics, 2012. **16**(5): p. 284-7.
18. Langfelder, P. and S. Horvath, *WGCNA: an R package for weighted correlation network analysis.* BMC Bioinformatics, 2008. **9**: p. 559.
19. Charoentong, P., et al., *Pan-cancer Immunogenomic Analyses Reveal Genotype-Immunophenotype Relationships and Predictors of Response to Checkpoint Blockade.* Cell Rep, 2017. **18**(1): p. 248-262.
20. Newman, A.M., et al., *Robust enumeration of cell subsets from tissue expression profiles.* Nat Methods, 2015. **12**(5): p. 453-7.

21. Mariathasan, S., et al., *TGFβ attenuates tumour response to PD-L1 blockade by contributing to exclusion of T cells.* Nature, 2018. **554**(7693): p. 544-548.
22. Auslander, N., et al., *Publisher Correction: Robust prediction of response to immune checkpoint blockade therapy in metastatic melanoma.* Nat Med, 2018. **24**(12): p. 1942.
23. Liu, C.J., et al., *GSCALite: a web server for gene set cancer analysis.* Bioinformatics, 2018. **34**(21): p. 3771-3772.
24. Li, J., et al., *Identification key genes, key miRNAs and key transcription factors of lung adenocarcinoma.* J Thorac Dis, 2020. **12**(5): p. 1917-1933.
25. Cotto, K.C., et al., *DGIdb 3.0: a redesign and expansion of the drug-gene interaction database.* Nucleic Acids Res, 2018. **46**(D1): p. D1068-d1073.
26. Uhlen, M., et al., *Proteomics. Tissue-based map of the human proteome.* Science, 2015. **347**(6220): p. 1260419.
27. Chen, D.S. and I. Mellman, *Oncology meets immunology: the cancer-immunity cycle.* Immunity, 2013. **39**(1): p. 1-10.
28. Yao, F., et al., *A targetable LIFR-NF-κB-LCN2 axis controls liver tumorigenesis and vulnerability to ferroptosis.* Nat Commun, 2021. **12**(1): p. 7333.
29. Li, Z.J., et al., *Artesunate synergizes with sorafenib to induce ferroptosis in hepatocellular carcinoma.* Acta Pharmacol Sin, 2021. **42**(2): p. 301-310.
30. Ye, F., et al., *HMGB1 regulates erastin-induced ferroptosis via RAS-JNK/p38 signaling in HL-60/NRAS(Q61L) cells.* Am J Cancer Res, 2019. **9**(4): p. 730-739.
31. Ghoochani, A., et al., *Ferroptosis Inducers Are a Novel Therapeutic Approach for Advanced Prostate Cancer.* Cancer Res, 2021. **81**(6): p. 1583-1594.
32. Demkow, U., *Neutrophil Extracellular Traps (NETs) in Cancer Invasion, Evasion and Metastasis.* Cancers (Basel), 2021. **13**(17).
33. Marra, F. and F. Tacke, *Roles for chemokines in liver disease.* Gastroenterology, 2014. **147**(3): p. 577-594.e1.
34. Hou, J., et al., *PTPROt maintains T cell immunity in the microenvironment of hepatocellular carcinoma.* J Mol Cell Biol, 2015. **7**(4): p. 338-50.
35. Zhang, W., et al., *IL-6 promotes PD-L1 expression in monocytes and macrophages by decreasing protein tyrosine phosphatase receptor type O expression in human hepatocellular carcinoma.* J Immunother Cancer, 2020. **8**(1).
36. Asbagh, L.A., et al., *The tyrosine phosphatase PTPRO sensitizes colon cancer cells to anti-EGFR therapy through activation of SRC-mediated EGFR signaling.* Oncotarget, 2014. **5**(20): p. 10070-83.
37. Wang, Z., et al., *CRHBP is degraded via autophagy and exerts anti-hepatocellular carcinoma effects by reducing cyclin B2 expression and dissociating cyclin B2-CDK1 complex.* Cancer Gene Ther, 2022.
38. Yang, K., et al., *Integrative analysis reveals CRHBP inhibits renal cell carcinoma progression by regulating inflammation and apoptosis.* Cancer Gene Ther, 2020. **27**(7-8): p. 607-618.

39. Jiang, C., et al., *MiRNA-15a-3p inhibits the metastasis of hepatocellular carcinoma by interacting with HMOX1.* Eur Rev Med Pharmacol Sci, 2020. **24**(24): p. 12694-12700.
40. Consonni, F.M., et al., *Heme catabolism by tumor-associated macrophages controls metastasis formation.* Nat Immunol, 2021. **22**(5): p. 595-606.
41. Chang, L.C., et al., *Heme oxygenase-1 mediates BAY 11-7085 induced ferroptosis.* Cancer Lett, 2018. **416**: p. 124-137.
42. Lin, H., et al., *EF24 induces ferroptosis in osteosarcoma cells through HMOX1.* Biomed Pharmacother, 2021. **136**: p. 111202.
43. Liu, F., et al., *Identification of FABP5 as an immunometabolic marker in human hepatocellular carcinoma.* J Immunother Cancer, 2020. **8**(2).
44. Seo, J., et al., *Fatty-acid-induced FABP5/HIF-1 reprograms lipid metabolism and enhances the proliferation of liver cancer cells.* Commun Biol, 2020. **3**(1): p. 638.
45. Field, C.S., et al., *Mitochondrial Integrity Regulated by Lipid Metabolism Is a Cell-Intrinsic Checkpoint for Treg Suppressive Function.* Cell Metab, 2020. **31**(2): p. 422-437 e5.
46. Esparza-Baquer, A., et al., *TREM-2 defends the liver against hepatocellular carcinoma through multifactorial protective mechanisms.* Gut, 2021. **70**(7): p. 1345-1361.
47. Molgora, M., et al., *TREM2 Modulation Remodels the Tumor Myeloid Landscape Enhancing Anti-PD-1 Immunotherapy.* Cell, 2020. **182**(4): p. 886-900 e17.
48. Tsai, T.J., et al., *Gelsolin-like Actin-capping Protein (CapG) Overexpression in the Cytoplasm of Human Hepatocellular Carcinoma, Associated with Cellular Invasion, Migration and Tumor Prognosis.* Anticancer Res, 2018. **38**(7): p. 3943-3950.
49. Westbrook, J.A., et al., *CAPG and GIPC1: Breast Cancer Biomarkers for Bone Metastasis Development and Treatment.* J Natl Cancer Inst, 2016. **108**(4).
50. Yun, D.P., et al., *Actin-capping protein CapG is associated with prognosis, proliferation and metastasis in human glioma.* Oncol Rep, 2018. **39**(3): p. 1011-1022.
51. Yi, L., et al., *Downregulation of NSD3 (WHSC1L1) inhibits cell proliferation and migration via ERK1/2 deactivation and decreasing CAPG expression in colorectal cancer cells.* Onco Targets Ther, 2019. **12**: p. 3933-3943.
52. Zhaojie, L., et al., *Gelsolin-like actin-capping protein has prognostic value and promotes tumorigenesis and epithelial-mesenchymal transition via the Hippo signaling pathway in human bladder cancer.* Ther Adv Med Oncol, 2019. **11**: p. 1758835919841235.
53. Cho, J., et al., *RGS2-mediated translational control mediates cancer cell dormancy and tumor relapse.* J Clin Invest, 2021. **131**(1).
54. Yang, T., et al., *The histone deacetylase inhibitor PCI-24781 impairs calcium influx and inhibits proliferation and metastasis in breast cancer.* Theranostics, 2021. **11**(5): p. 2058-2076.
55. Low, J.S., et al., *A Genome Wide Study of Copy Number Variation Associated with Nasopharyngeal Carcinoma in Malaysian Chinese Identifies CNVs at 11q14.3 and 6p21.3 as Candidate Loci.* PLoS

One, 2016. **11**(1): p. e0145774.

56. Sangro, B., et al., *A clinical trial of CTLA-4 blockade with tremelimumab in patients with hepatocellular carcinoma and chronic hepatitis C.* J Hepatol, 2013. **59**(1): p. 81-8.
57. El-Khoueiry, A.B., et al., *Nivolumab in patients with advanced hepatocellular carcinoma (CheckMate 040): an open-label, non-comparative, phase 1/2 dose escalation and expansion trial.* Lancet, 2017. **389**(10088): p. 2492-2502.
58. *Correction to Lancet Oncol 2021; 22: 977-90.* Lancet Oncol, 2021. **22**(8): p. e347.
59. Kuang, D.M., et al., *Activated monocytes in peritumoral stroma of hepatocellular carcinoma foster immune privilege and disease progression through PD-L1.* J Exp Med, 2009. **206**(6): p. 1327-37.
60. Wu, K., et al., *Kupffer cell suppression of CD8+ T cells in human hepatocellular carcinoma is mediated by B7-H1/programmed death-1 interactions.* Cancer Res, 2009. **69**(20): p. 8067-75.
61. Shi, F., et al., *PD-1 and PD-L1 upregulation promotes CD8(+) T-cell apoptosis and postoperative recurrence in hepatocellular carcinoma patients.* Int J Cancer, 2011. **128**(4): p. 887-96.
62. Li, H., et al., *Tim-3/galectin-9 signaling pathway mediates T-cell dysfunction and predicts poor prognosis in patients with hepatitis B virus-associated hepatocellular carcinoma.* Hepatology, 2012. **56**(4): p. 1342-51.
63. Li, F.J., et al., *Expression of LAG-3 is coincident with the impaired effector function of HBV-specific CD8(+) T cell in HCC patients.* Immunol Lett, 2013. **150**(1-2): p. 116-22.
64. Alu, A., et al., *The role of lysosome in regulated necrosis.* Acta Pharm Sin B, 2020. **10**(10): p. 1880-1903.
65. Zhang, W., et al., *The progress and perspective of nanoparticle-enabled tumor metastasis treatment.* Acta Pharm Sin B, 2020. **10**(11): p. 2037-2053.
66. Robertson, K.D., *DNA methylation and human disease.* Nat Rev Genet, 2005. **6**(8): p. 597-610.
67. Ozaki, Y., et al., *DNA methylation changes at TREM2 intron 1 and TREM2 mRNA expression in patients with Alzheimer's disease.* J Psychiatr Res, 2017. **92**: p. 74-80.
68. Long, J., et al., *DNA methylation-driven genes for constructing diagnostic, prognostic, and recurrence models for hepatocellular carcinoma.* Theranostics, 2019. **9**(24): p. 7251-7267.
69. Hlady, R.A., et al., *Genome-wide discovery and validation of diagnostic DNA methylation-based biomarkers for hepatocellular cancer detection in circulating cell free DNA.* Theranostics, 2019. **9**(24): p. 7239-7250.
70. Bassaganyas, L., et al., *Copy-Number Alteration Burden Differentially Impacts Immune Profiles and Molecular Features of Hepatocellular Carcinoma.* Clin Cancer Res, 2020. **26**(23): p. 6350-6361.
71. Bruix, J. and M. Sherman, *Management of hepatocellular carcinoma.* Hepatology, 2005. **42**(5): p. 1208-36.
72. Llovet, J.M., et al., *Advances in targeted therapies for hepatocellular carcinoma in the genomic era.* Nat Rev Clin Oncol, 2015. **12**(7): p. 408-24.

73. Liu, D., et al., *Radiation Dosimetry of Whole-Body Dual-Tracer 18F-FDG and 11C-Acetate PET/CT for Hepatocellular Carcinoma.* J Nucl Med, 2016. **57**(6): p. 907-12.
74. He, X., et al., *Cephalosporin antibiotics specifically and selectively target nasopharyngeal carcinoma through HMOX1-induced ferroptosis.* Life Sci, 2021. **277**: p. 119457.
75. Chen, X., et al., *Role of Exosomes in Immune Microenvironment of Hepatocellular Carcinoma.* J Oncol, 2022. **2022**: p. 2521025.

Supplementary Information

Supplementary Tables and Figures are not available with this version.

Figures

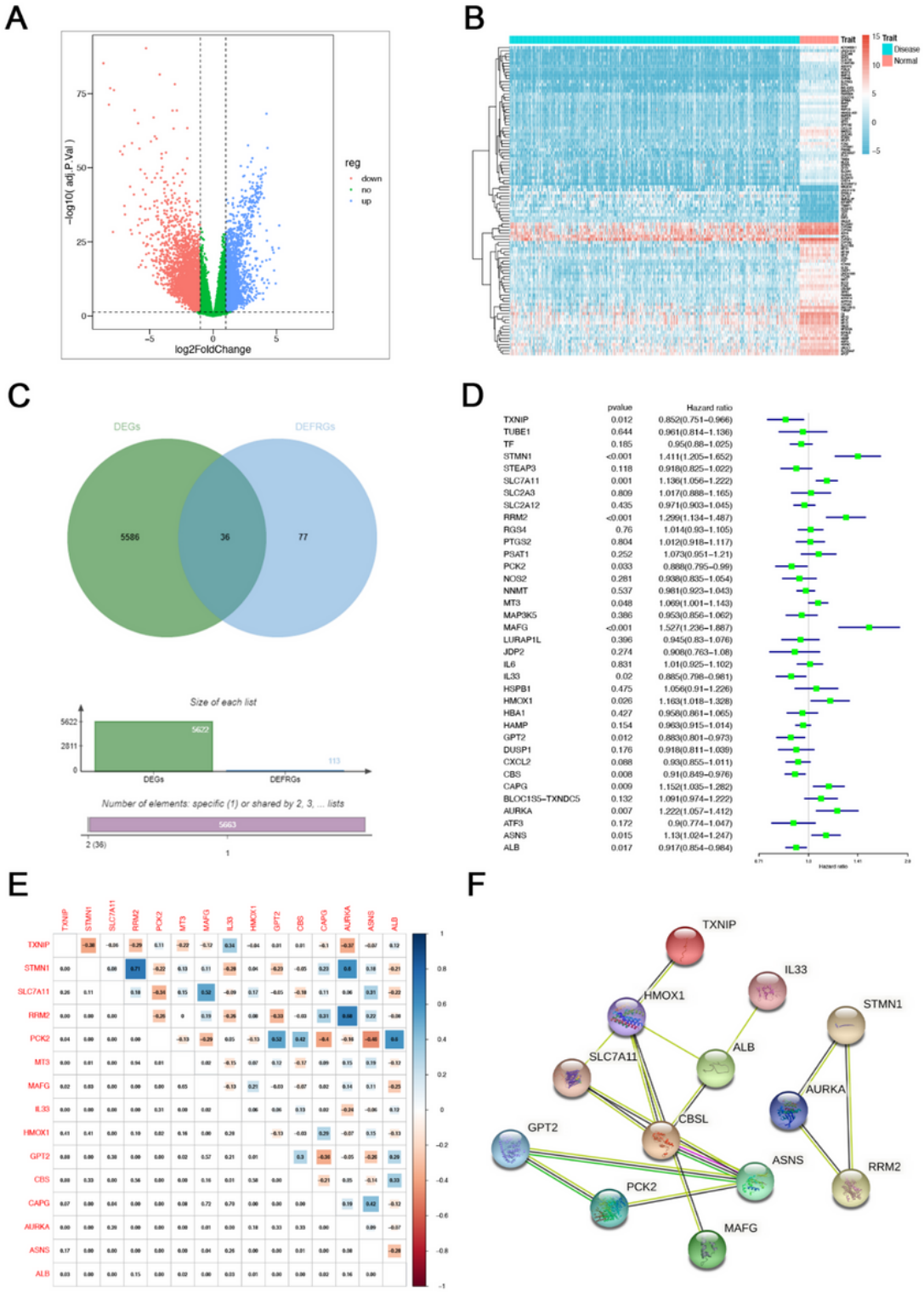

Figure 1

Screening of prognosis-related differential ferroptosis genes (DEFRGs) in HCC. (**A**) Volcano plot of DEGs between the non-tumorous and HCC groups. The up-and down-regulated DEGs are labelled in blue and red respectively. (**B**) Expression profiles of the top 100 DEGs. (C) Venn diagram of DEFRGs. (**D**) DEFRGs remarkably correlated with HCC prognosis. (**E**) Heat map of correlation between prognostic DEFRGs. (**F**) Protein-protein interaction network of prognostic DEFRGs.

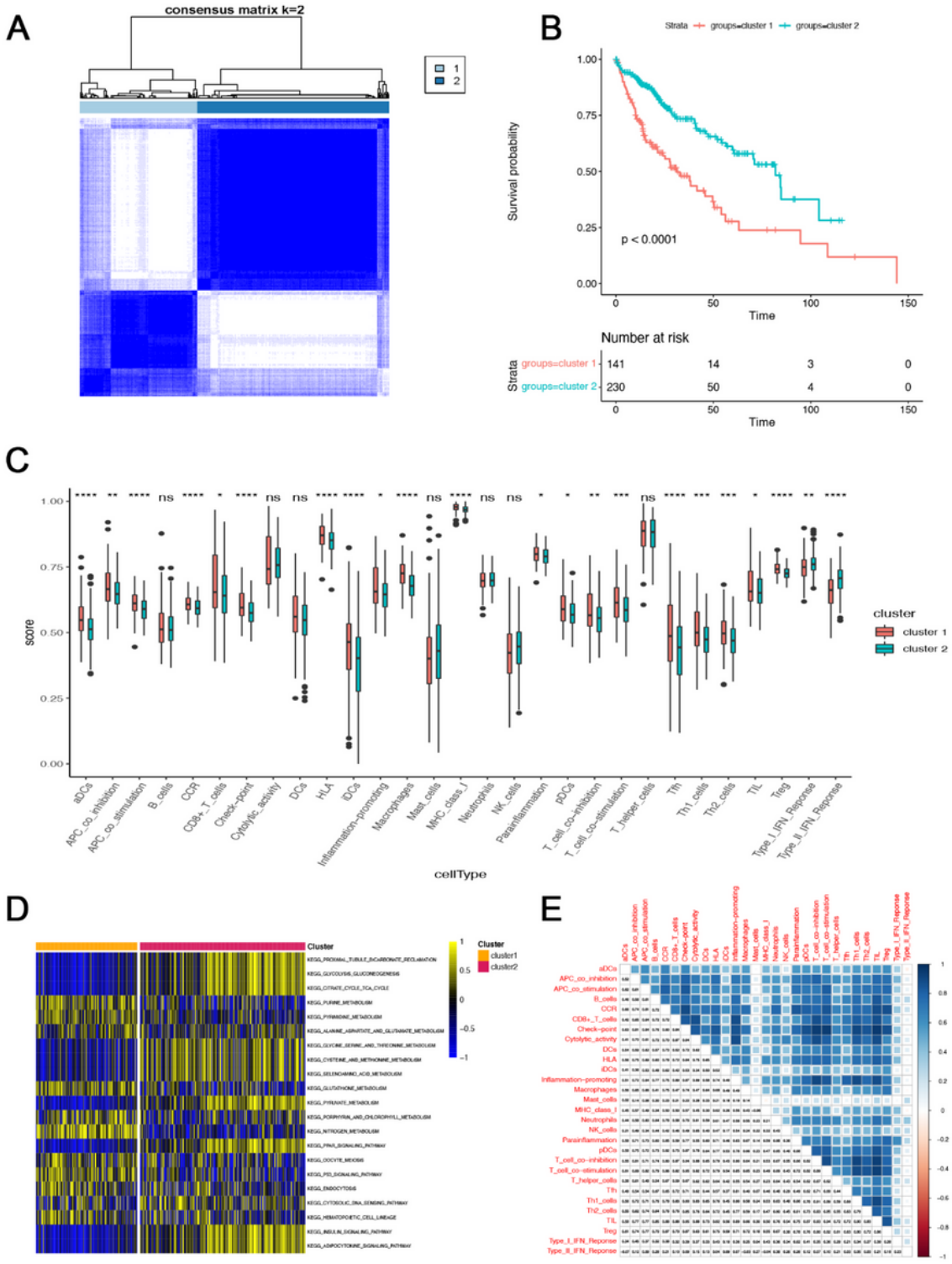

Figure 2

Prognostic ferroptosis genes cluster analysis and differential immune cell identification. (**A**) Patients were stratified into two clusters by ConsensusClusterPlus. (**B**) Kaplan-Meier survival curves of OS in two clusters. (**C**) The ssGSEA scores of immune cells along with immune functions in two clusters. (**D**) Significant variations of the KEGG pathways in two clusters. (**F**) Correlation heatmap of immune cells with the immune functions.

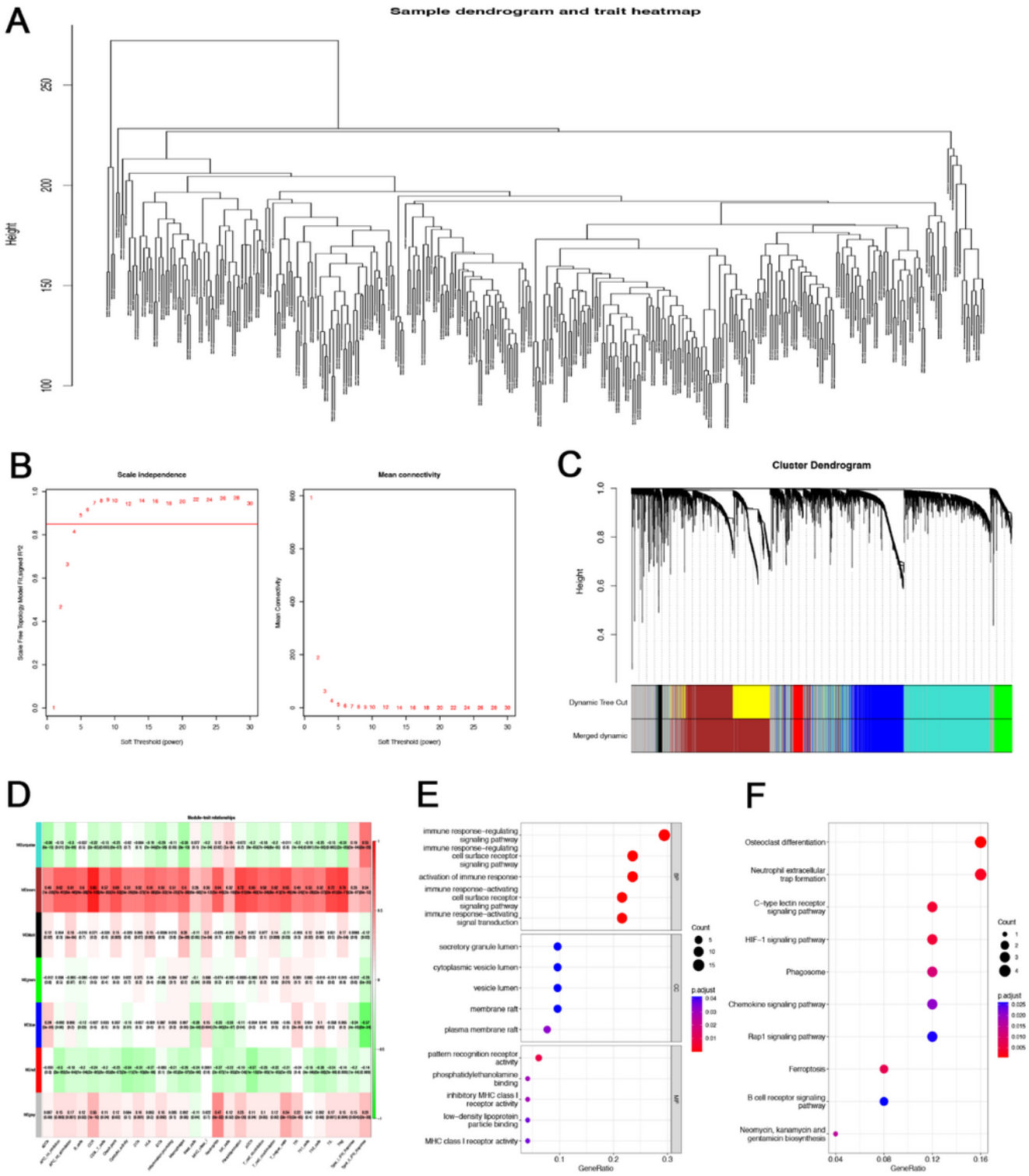

Figure 3

WGCNA analysis. (**A**) Cluster dendrogram of 370 samples. (**B**) The scale-free fit index for soft-thresholding power. (**C**) Hierarchical clustering dendrogram of recognized co-expressed genes in modules in HCC. Each colored row refers to a color-coded module containing a set of highly linked genes. A total of 7 modules was identified in HCC. (**D**) A heat map exhibiting relationships of the gene modules with the

immune signature. Enrichment results for the top five GO (**E**) and top ten KEGG (**F**) of ferroptosis-immune microenvironment-related genes.

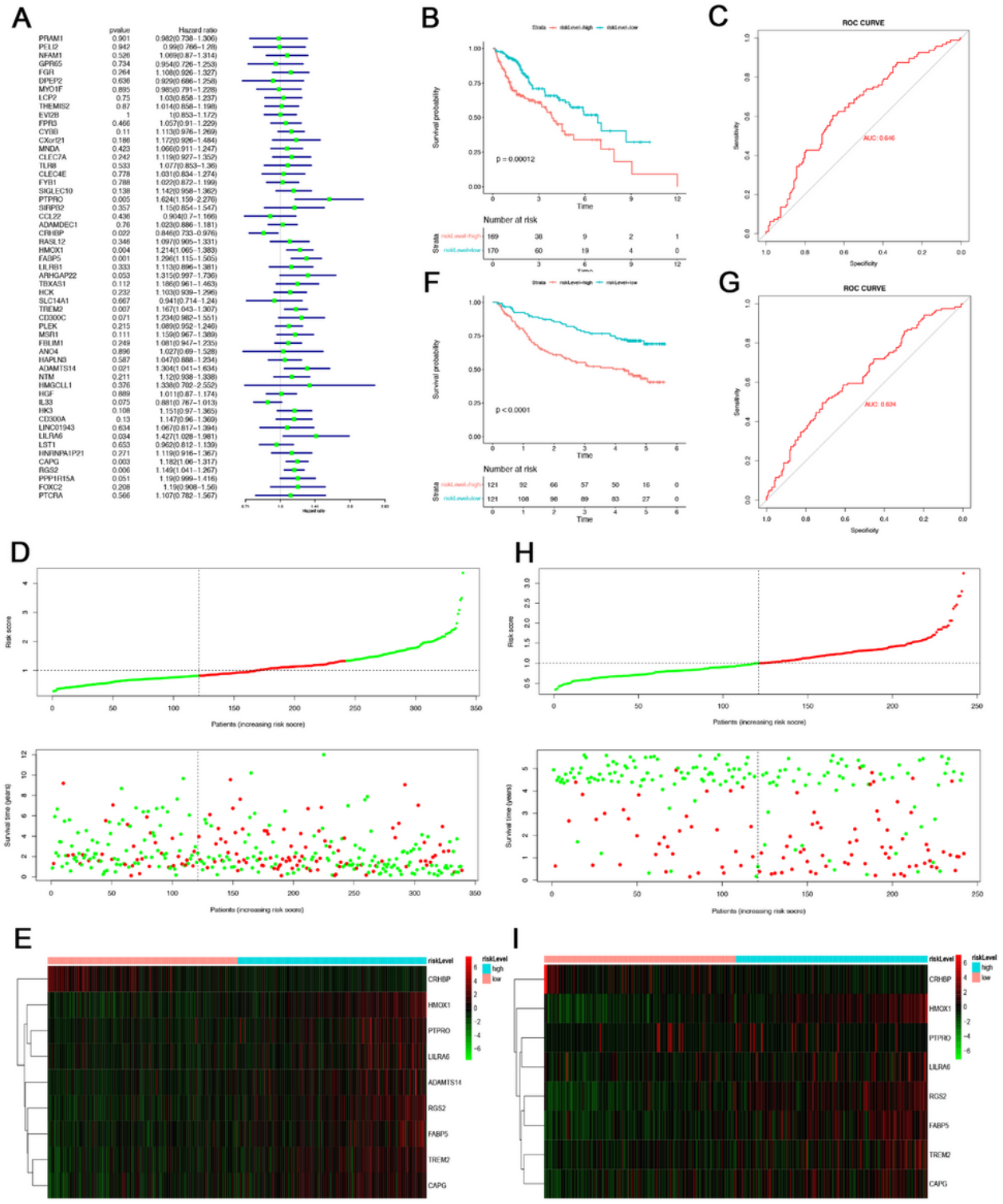

Figure 4

Generation and verification of risk score model in the TCGA, as well as GSE14520 cohort. (**A**) Univariate Cox assessment for authenticating prognosis-linked genes. (**B**) K-M curve of TCGA data set. (**C**) ROC

curve for forecasting OS in TCGA data set. (**D**) Distribution of the risk score and survival status of individuals with HCC in TCGA cohort. (**E**) Expression profiles of nine FIMRGs in individuals with HCC in TCGA cohort. (**F**) K-M curve of GSE14520 cohort. (**G**) ROC curves for forecasting OS in GSE14520 cohort. (**H**) Distribution of the risk score d and survival status of individuals with HCC in GSE14520 cohort. (I) Expression profiles of nine FIMRGs in HCC patients in GSE14520 cohort.

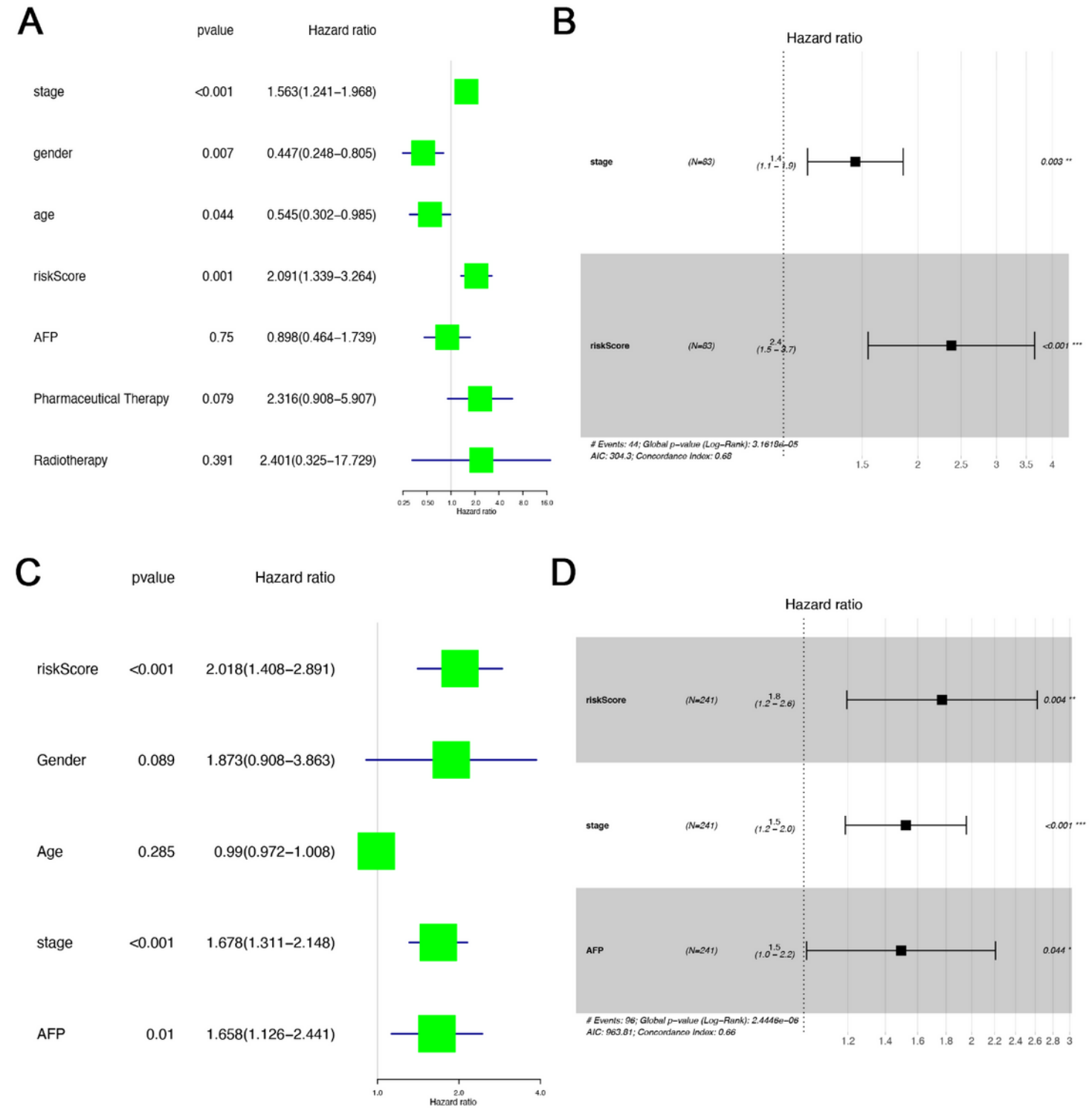

Figure 5

Independent prognostic analysis. Univariate (**A**) along with multivariate (**B**) Cox regression assessment of the clinical features and risk score in TCGA data set. Univariate (**C**) along with multivariate (**D**) Cox regression assessment of the clinical variables and risk score in GSE14520 cohort.

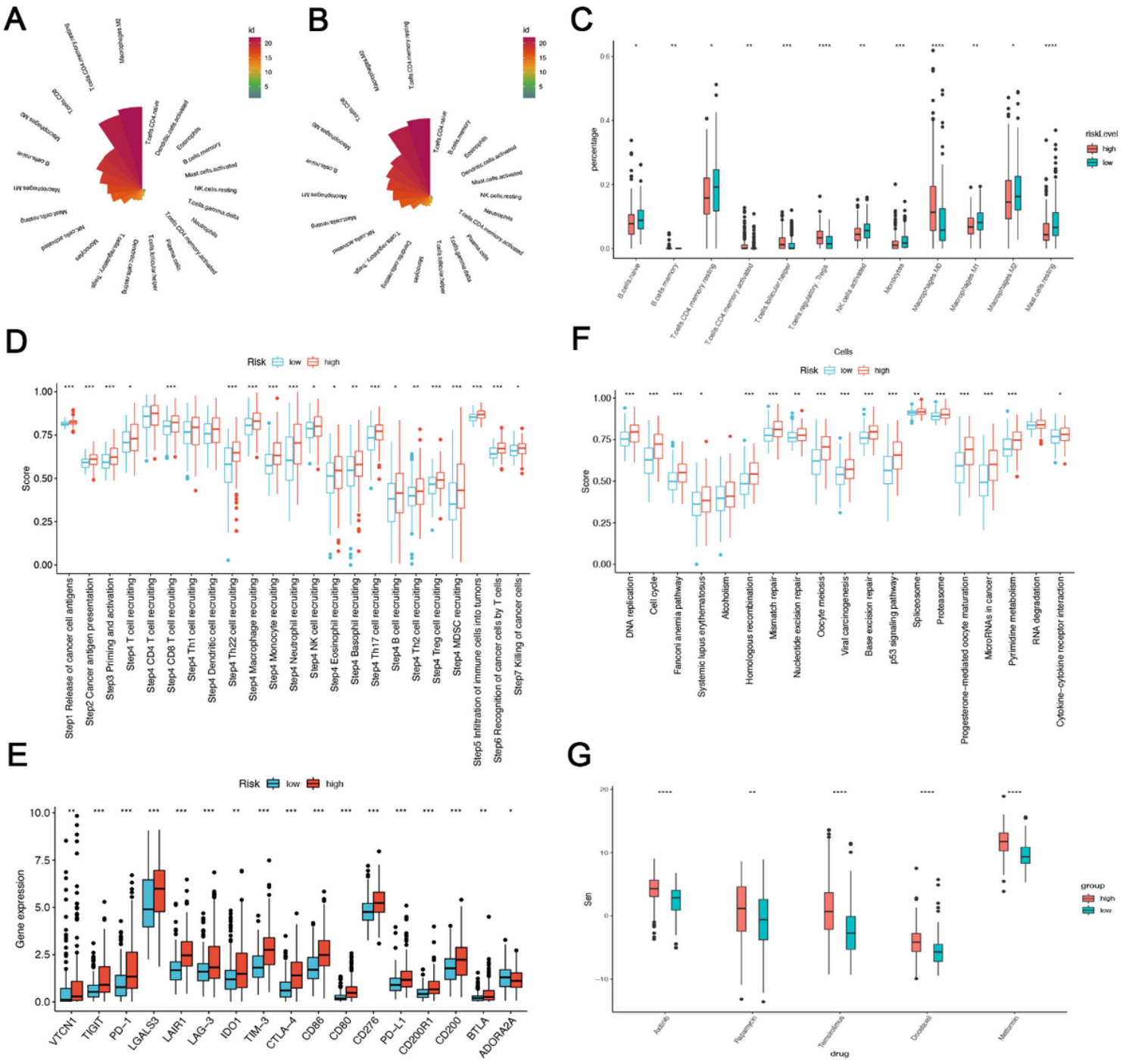

Figure 6

The profiling of tumor immune microenvironment in the high-HCC and low-HCC risk groups. Comparison of immune cell fractions by CIBERSORT in the high-HCC risk group (**A**) and low-HCC risk group (**B**) of the TCGA data set. (**C**) Immune cell subset differences in high-HCC and low-HCC risk groups. (**D**) Distinction

between high-HCC and low-HCC risk groups at diverse stages of the cancer immunity cycle. (**E**) Immune checkpoint differences between high-HCC and low-HCC risk populations. (**F**) Differences in immunotherapy-predicted cascade enrichment scores between high-HCC and low-HCC risk groups. (**G**) Distinction in chemotherapy drug sensitivity between the high-HCC and low-HCC risk groups.*p < 0.05 **p < 0.01 ***p < 0.001.

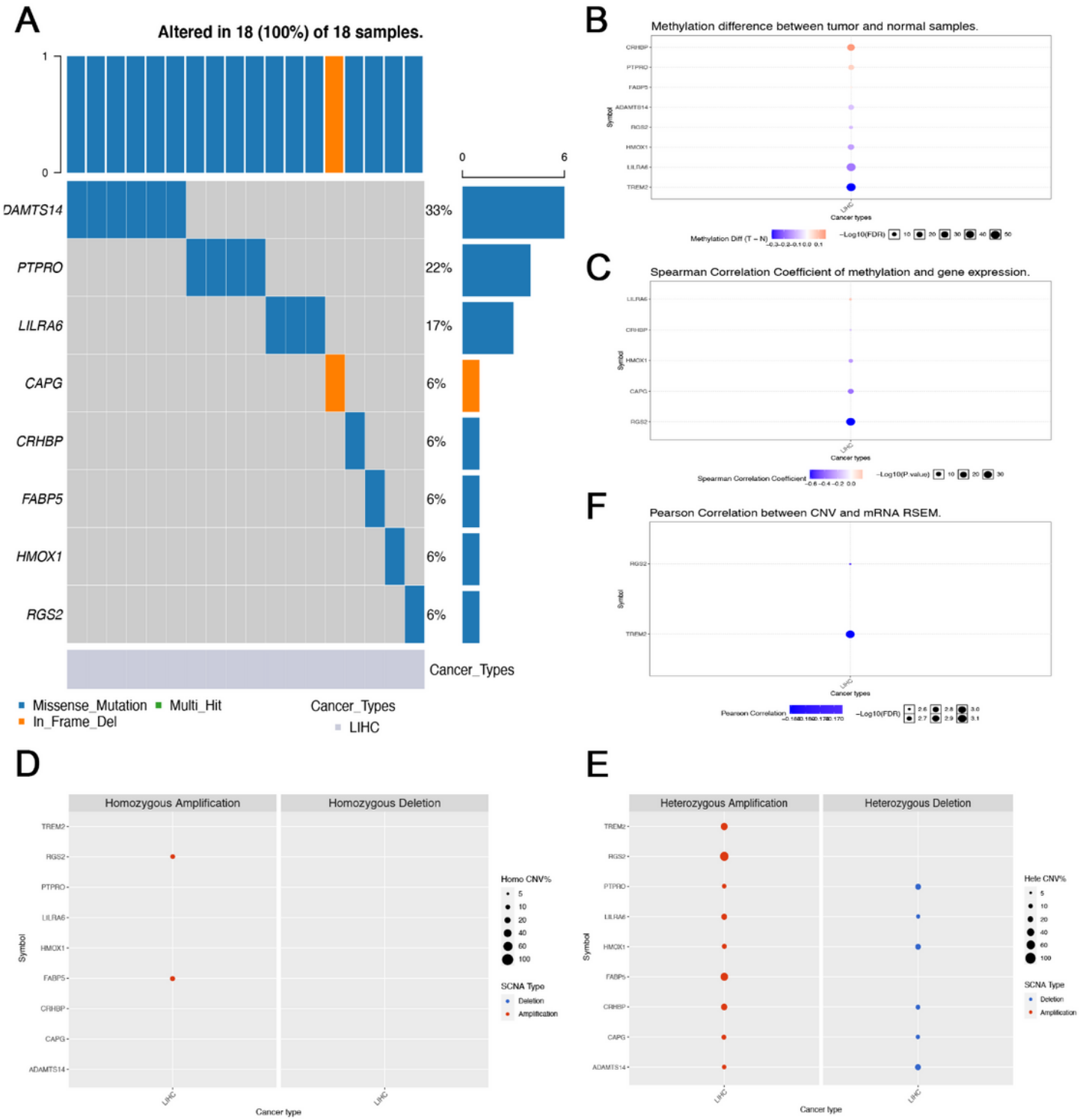

Figure 7

Multi-omics assessment of nine prognostic genes in TCGA data set by GSCALite. (**A**) Mutation waterfall map of eight genes. (**B**)Methylation difference of prognostic genes between tumor and non-tumorous samples. (**C**)Spearman correlation between methylation and gene expression. (**D-F**)CNV analysis of nine prognostic genes.

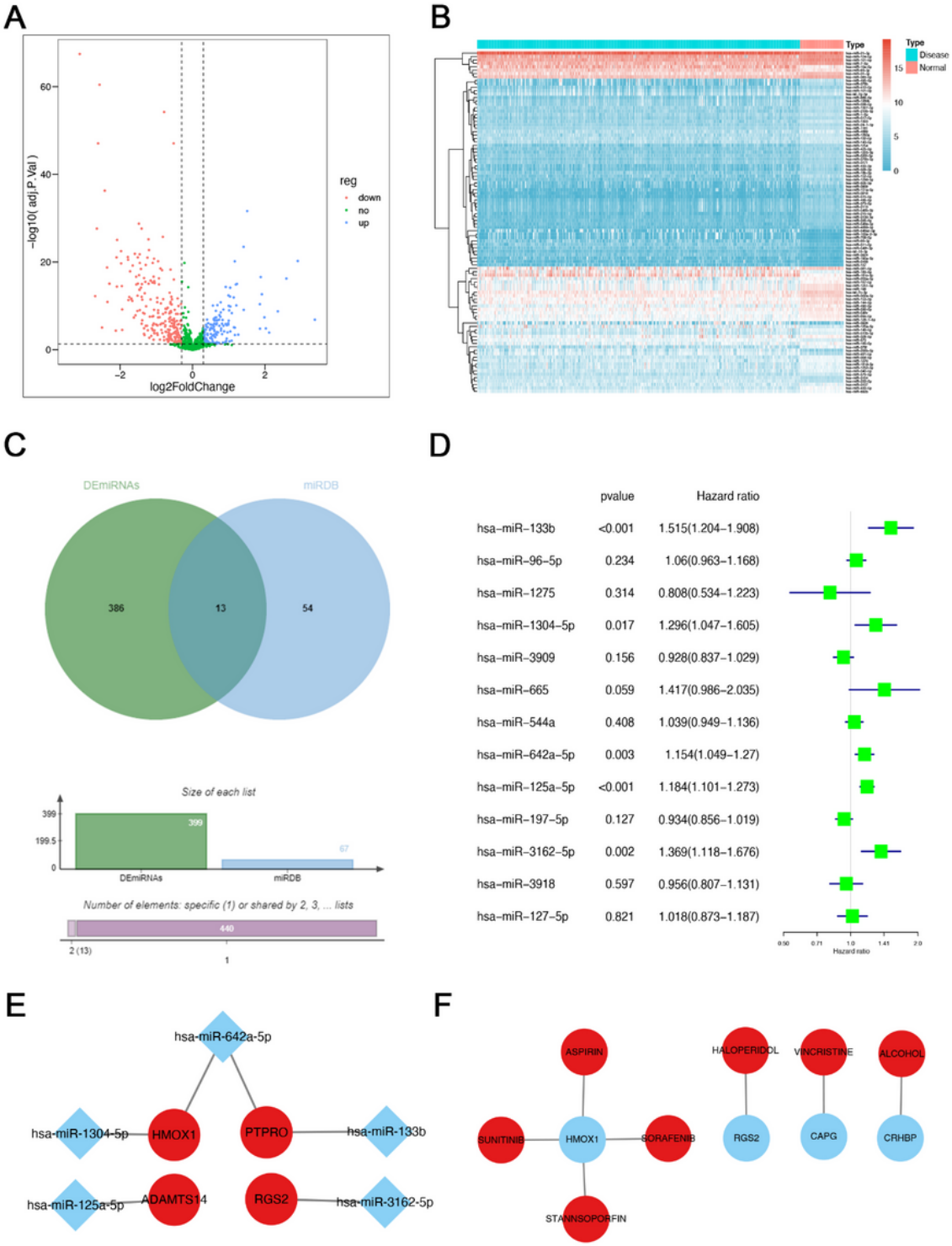

Figure 8

MiRNA-mRNA regulatory network construction and drug prediction. (**A**) Volcano plot of differential expressed miRNAs (DE-miRNAs) between the normal and HCC groups. The up-and-down-regulated DE-miRNAs are respectively designated in blue and red. (**B**) Expression patterns of the top 100 DE-miRNAs. (**C**)Venn diagram of the miRbase predicted target miRNAs crossed with DE-miRNAs. (**D**) Univariate analysis of the crossover miRNAs. (**E**) MiRNA-mRNA regulatory network diagram. (**F**) Potential drug relationship prediction for model genes.

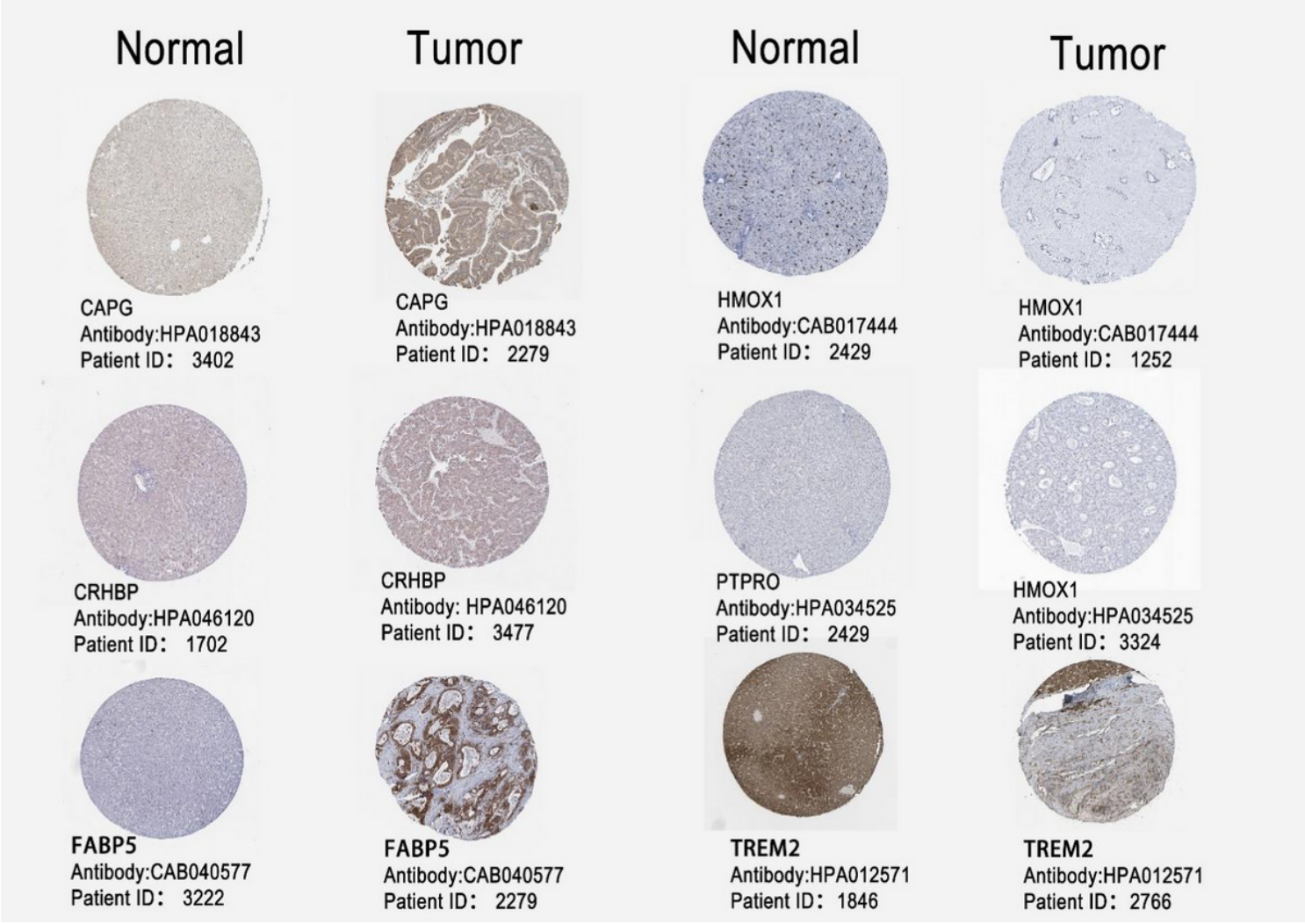

Figure 9

The histological expression of FIMRGs. The category of the tissue specimen is indicated at the top of the figure. The name of the genes, the type of antibody used in immunohistochemistry, and the patient ID of the tissue specimen are shown at the bottom of each image.